EFFECT OF PROCESSING PARAMETERS ON THE DENSITY AND MICROSTRUCTURE OF DIRECT LASER SINTERED Al-12Si POWDERS.

E.O.Olakanmi[a], R.F.Cochrane[a], K.W.Dalgarno[b].
a Institute for Materials Research, University of Leeds, LS2 9JT.
b School of Mechanical and Systems Engineering, Newcastle University, NE1 7RU, UK.

Abstract

The effect of processing parameters on the sintering behaviour of gas atomised Al-12Si powders has been investigated. Laser power, scanning rate, scan spacing and layer thickness are found to control the densification and the resultant microstructural characteristics of the laser sintered parts. It was found that sintered density increased as the energy density increased reaching a maximum of 80.2% at an energy input per unit volume of 67 J mm^{-3}. For parts produced with a slightly lower power density (50 J mm^{-3}), the microstructure consisted of fine dendrites with interconnected porosity while parts fabricated with a slightly higher power density (100 J mm^{-3}) were noted to have a preponderance of coarse dendrites with a discontinuous network of irregular shaped pores surrounded by a fully dense aluminium-silicon matrix.

Keywords: Al-12Si alloyed powder; Microstructure; Energy Density; Scanning Electron Microscopy (SEM); Densification.

1. Introduction

The specialty of the direct selective laser sintering (SLS) process has been identified as one of the most promising areas for the production of engineering components. This is because it does not require moulds to produce intricate geometries and eliminates the post-processing steps thereby resulting in the shortening of the production cycle as well as the reduction of production costs. For example, studies on the direct SLS of high speed steels (HSS) have been carried out [1-7]; while the processability of stainless steel powders had been investigated [8-9]. The role of laser sintering parameters, powder particle morphology, and powder oxygen content in the sintering response of laser sintered M3/2 and M2 high speed steel powders had been described [1-4]. The inference from these studies is that the transition from solid phase sintering to liquid phase sintering via full melting/solidification with increasing laser power at low scanning rates is the underlying mechanism guiding the SLS process. Marangoni flow in the melt pool was discovered to have affected the morphology of the sintered tracks at high laser power and low scanning rates. The agglomerate sizes increased with increasing laser power or decreasing scan rates. Moreover, it was observed that powder particle size less than 38μm had low sintered density as a result of high oxygen level.

Corresponding author, Tel Direct (0113) 343 2359; Fax: (0113) 343 2384
E-mail address: r.f.cochrane@leeds.ac.uk (Dr R.F.Cochrane)

It had been suggested that the surface tension gradient is a significant factor causing the spherodisation of the tracks or the break up of the liquid cylinder [1-4]. The energy exchange in the SLS of titanium powders via the application of the principle of the conventional coupling between laser and material as well as the phenomenon of the gray body behaviour of granulated media had been well elucidated [10]. Three key repetition domains, namely high repetition rate domain, lower domain and intermediate domain, were identified with respect to pulse energy and heating effects [10]. It was concluded that the intermediate domain constitutes the optimal processing window characterised by fast and localised heating which minimises the plasma effect [10]. Furthermore, the influence of laser parameters on the materials properties of laser sintered titanium and platinum-alloyed powders were investigated [11]. It was established that with the appropriate laser energy deposition in the powder bed, the degree of porosity, the density, as well as the crystalline microstructure can be controlled to meet the requirements of the finished work piece [11]. The influence of process parameters and heat treatment on the microstructure of direct laser fabricated TiAl alloy samples was investigated [12]. The findings from this study revealed that a variety of microstructures, ranging from cellular to columnar to dendritic morphologies, is obtainable upon the variation of the laser power and scanning speed. Furthermore, heterogeneous and finer microstructure were imparted to direct laser fabricated samples on comparison with the conventionally processed engineering parts made of titanium alloys. Subsequent heat treatment of the direct laser fabricated samples eventually resulted in the elimination of the compositional heterogeneity and coarseness of the samples [12].

No systematic work on the effect of processing parameters on the microstructural development of aluminium alloys employing SLS has been published to date. The aim of this work is to investigate the impact of the laser processing parameters on the densification and attendant microstructural characteristics of aluminium powder parts produced directly from the SLS process using a continuous wave CO_2 laser beam. The microstructure of direct laser fabricated Al-12Si parts is characterised as a function of the process parameters.

2. Experimental procedure.

The starting material was inert gas atomized 45-75μm Al-12Si powder (spherical shaped particle), supplied by ALPOCO Limited. The loose apparent density, tap density, and flowability of the powder were determined according to the MPIF standard tests 01, 46 and 03 methods. A Philips XL30 ESEM Scanning Electron Microscope (SEM) with link Systems EDX and image capture accessories was employed to observe the particle shape. The chemical composition of the powder as supplied by ALPOCO is presented in Table 1. Multiple layer samples were produced in Al-12Si powder by a Synrad 240W CO_2 laser of 0.6 mm beam diameter having Gaussian profile. The laser processing parameters were used over the following ranges: laser power (100-200 W), scan rate (80-200 mms[-1]), scan spacing 0.1-0.3 mm, and layer thickness 0.25-1.00 mm. The description of the experimental apparatus and the procedure adopted for building multiple layer samples are given in [6]. The density of the fabricated samples was measured by using the volumetric method according to [6]. The processing condition for each sample was repeated at least

twice and the density mean value recorded twice. Samples for metallographic examination were prepared and etched in dilute Keller's reagent.

Table 1: Elemental Composition of the Powdered Samples as Supplied by ALPOCO (Weight %).

Powdered Samples	Aluminium	Silicon	Oxygen	Iron	Copper
Al-12Si	88.40	12.1	-	0.36	0.08

3. Results.

3.1: Powder Characterisation.

Table 2: Powders' Characterisation.

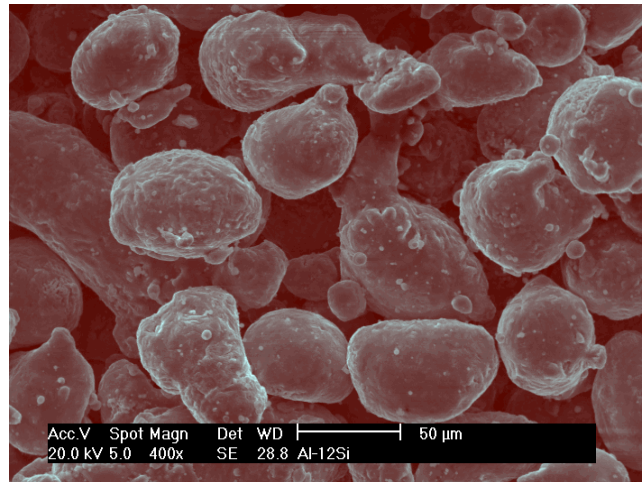|	Loose Apparent Density (gcm^{-3})	Tapped Density (gcm^{-3})	Flowability (s/50g)
Al-12Si	1.4347	1.7238	4.90

Figure 1: The spherical particle shape of the Al-12Si powder.

Table 2 and Figure 1 above indicate that both loose apparent and tapping densities of the powder are function of the powder's characteristics such as particle shape, particle porousity and particle size distribution. A comparison of loose apparent and tapping densities shows that 20.15% percentage increase in density was obtained upon the tapping of Al-12Si powder. This is explained by the fact that its spherical particles are suspected to have packed without bridging or arching, thus creating empty spaces, as the particles move easily past each other because of their smooth surfaces.

3.2: Effect of SLS Processing Parameters on the Sintered Density of Al-12Si Powder.

Figures 2, 3, and 4 show the effects of the direct laser sintering process parameters on the sintered density of the Al-12Si powder. Generally, as shown in Figure 2, an increase in the laser scanning speed results in the reduction of the sintered density of Al-12Si powder over the range of laser power studied 100 W-200 W. A consideration of the relationship between the sintered density and the laser power of Al-12Si powder shows that sintered density increases as the laser power increases. For instance, densities of 65.9%, 70.8%, and 80.2% were obtained when laser powers of 100 W, 150 W, and 200 W respectively were employed for SLS at the scanning rate of 120 mms^{-1} (Figure 2). Figure 2 also shows that the densities of Al-12Si sample sintered at 200 W (71.5% and 71.3%) are found to lie between the density values obtained at 100 W (70.4% and 66.3%) and 150 W (72.9% and 73.6%) for scanning rates of 80 and 100 mms^{-1}. The normal expectation is that the density values obtained for 200 W over these scanning rates should be higher than those values obtained at both 100 W and 150 W because of the likelihood of the formation of greater quantity of liquid phase that promotes densification at higher laser power for which greater energy density is being deposited on the powder bed. As the scanning rates increase over the range of 120 mms^{-1} to 200 mms^{-1}, density values obtained for 200 W are indeed found to be higher than those obtained for 150 W and 100 W for corresponding scanning rates. Furthermore, Figures 3 and 4 reveal that there exist inverse relationships between the sintered density and both scan spacing and layer thickness.
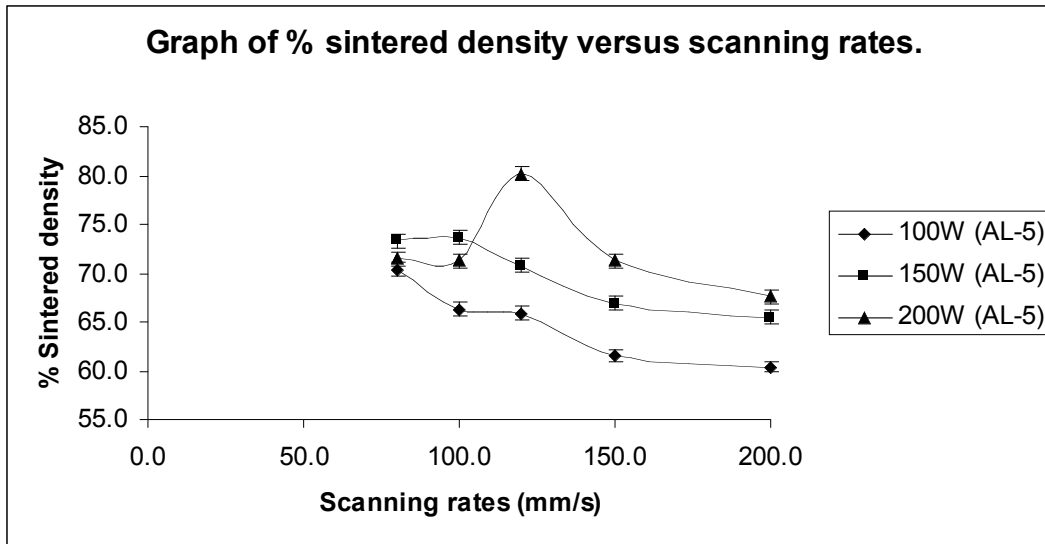

Figure 2: Variation of sintered density of Al-12Si powder with the scan rates when laser power varies between 100 W -200 W and scan spacing and layer thickness were held fixed at 0.1mm and 0.25mm respectively.
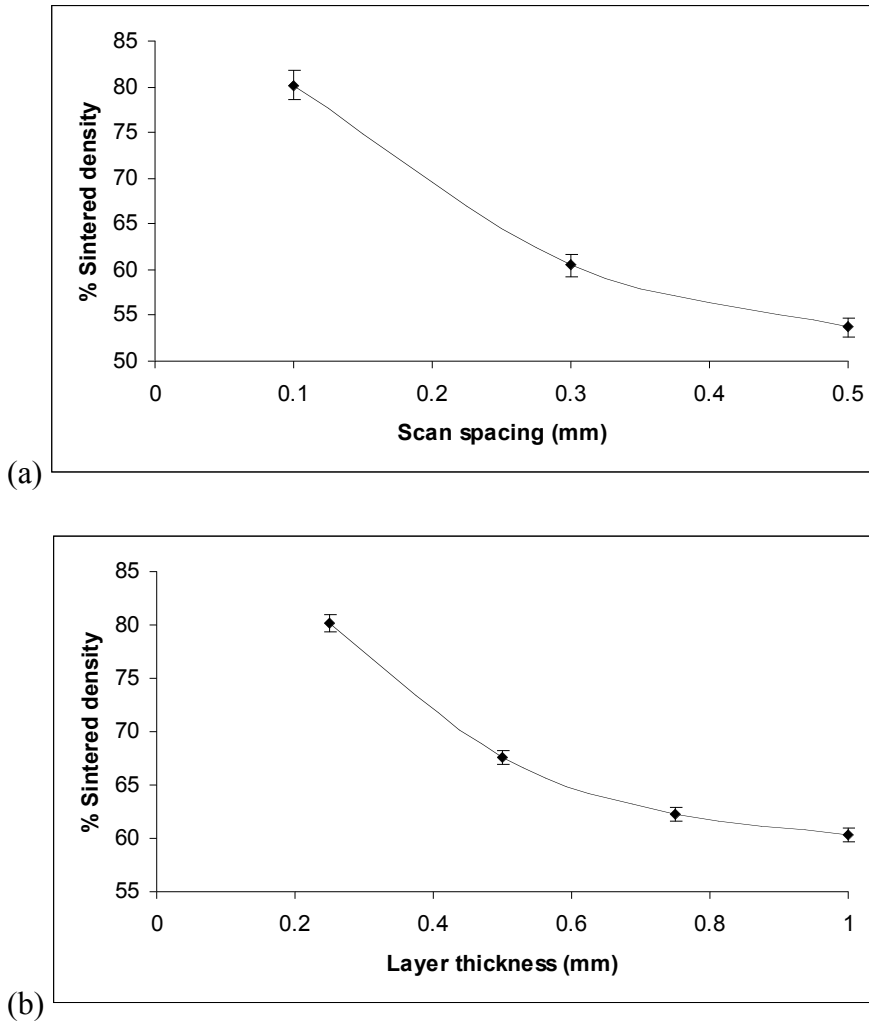
(a)

(b)

Figure 3: Variation of the sintered density of Al-12Si powder with (a) scan spacing and (b) layer thickness.

3.3: Effect of SLS Processing Parameters on the Microstructure of Al-12Si Powder.

Figure 4 shows the nature of the pore structures obtained in direct laser sintered Al-12Si specimens as a function of the processing conditions. Although in each case, the microstructures contain small pores, the connectivity and orientation of pores are largely dependent on the choice of processing parameters. For instance, elongated pores which are nearly perpendicular to the building direction were found in a sample fabricated with a laser power of 200 W; scan rates of 120 mms[-1]; scan spacing of 0.1 mm and layer thickness of 0.25 mm (Figure 4 (a)). The eutectics are fully dense and consist of dendrites which are oriented nearly perpendicular to the build direction. Upon increasing the scan spacing to 0.5 mm, it was discovered that the orientation of the pores becomes undefined relative to the building direction (Figure 4 (b)). The eutectics obtained for the scan spacing of 0.5mm are observed not to have been as fully dense as the one obtained for the sample made with scan spacing of 0.1 mm. It is easily discernible that the pore sizes in

the sample made with scan spacing of 0.5 mm are larger than the pore sizes of the sample made with scan spacing of 0.1 mm.
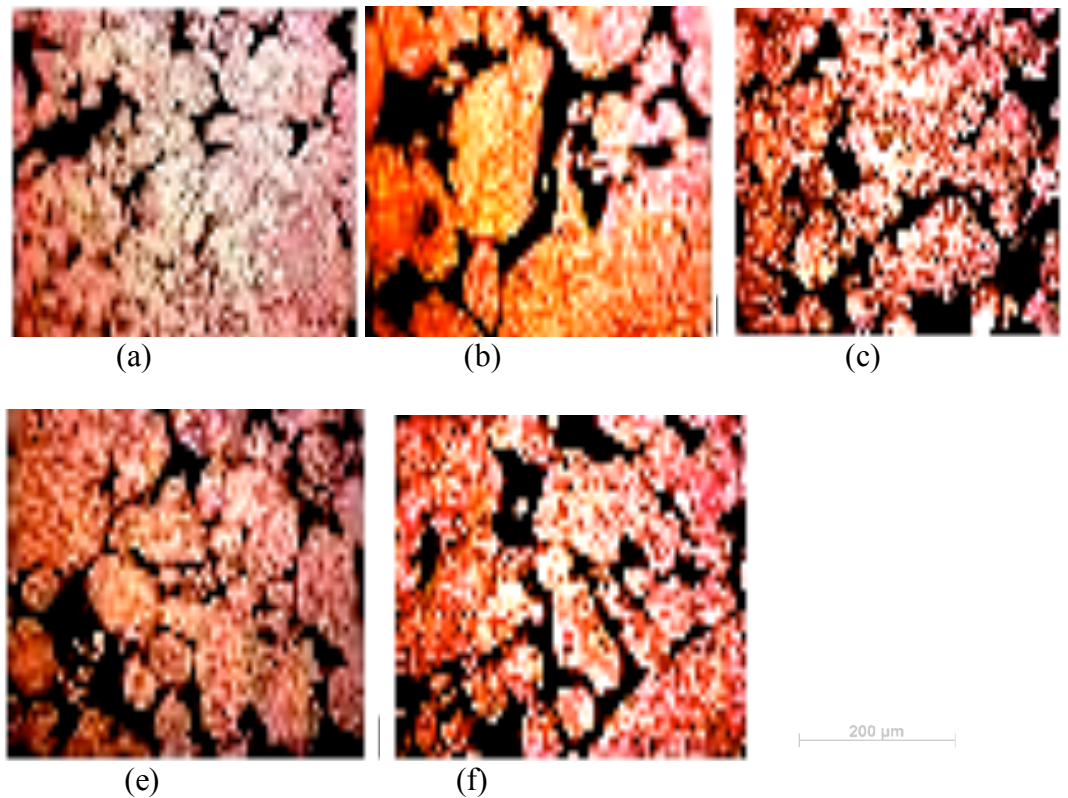

Figure 4: Polished section of direct laser sintered Al-12Si powder revealing the pore structures with varying processing conditions: (a) laser power 200 W; scan rates 120 mms^{-1}; layer thickness 0.25 mm; and scan spacing 0.1 mm (b) laser power 200 W; scan rates 120 mms^{-1}; layer thickness 0.25 mm; and scan spacing 0.5 mm (c) laser power 200 W; scan rates 120 mms^{-1}; layer thickness 1.0 mm; and scan spacing 0.1 mm (d) laser power 200 W; scan rates 200 mms^{-1}; layer thickness 0.25 mm; and scan spacing 0.1 mm (e) laser power 100 W; scan rates 120 mms^{-1}; layer thickness 0.25 mm; and scan spacing 0.1 mm.

The pore sizes correlate well with sintered density. The density was markedly higher (80.2%) for the sample made with the scan spacing of 0.1 mm than that obtained for the sample made with a scan spacing of 0.5 mm (53.7%). The findings so far indicate that increasing the scan spacing leads to an increase in pore sizes, less dense eutectics and less oriented pores. Furthermore, similar results were obtained with increasing layer thickness (Figure 4c), increasing scan rates (Figure 4d), and decreasing laser power (Figure 4e).

Figures 5, 6, and 7 show optical micrographs of laser sintered Al-12Si powder processed at energy densities of 100 Jmm^{-3}, 67 Jmm^{-3}, and 50 Jmm^{-3} respectively. Black regions in the micrographs are an indication of the presence of pores while the grey region corresponds to the sintered mass. The pores are found to be responsible for a significant decrease in the densities of the sintered parts.
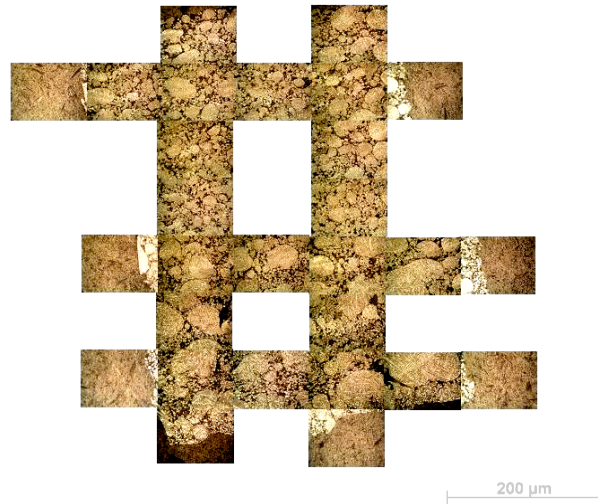
Figure 5: Sections through the micrograph of AL-5 (200 W-80 mms^{-1}) generated by 100 Jmm^{-3}.

Under these conditions, a coarse eutectic microstructure is observed as shown in Figures 8(a) and (b) for samples fabricated with 100Jmm^{-3}. The microstructure contains small pores (Figure 5). Furthermore no continuous network of pores was observed; rather, irregular shaped pores with no orientation to the building direction, surrounded by a fully dense aluminium-silicon matrix are formed. As the energy density is reduced to 67 Jmm^{-3} (Figure 6), consequently, a finer microstructure as shown in Figures 8(c) and (d) results from the processing condition. Here, the finer dendritic microstructure and the interdendritic porosity found could be attributed to the shrinkage which occurs during solidification and/or with the presence of some entrapped argon. As the energy density is reduced to 50 Jmm^{-3}, (Figure 7) it can be seen that the heat input is just enough to sinter the powder. The consequence of this is that the dendritic microstructure can be seen to have become still finer but the interconnectivity of the porosity increases. Figure 8 reveals that, for all samples, the dendrites become coarser and porosity increases towards the bottom part of the sintered samples.

4.0: Discussion:

The most important parameter that affects the density and microstructure of direct laser sintered materials is the energy density. Energy density during the laser sintering process is defined by the following relationship:

$$E = P / (V) \text{ x } (d) \text{ x } (h)\ldots\ldots\ldots\ldots\ldots\ldots\ldots\ldots.(1)$$

Where E is the incident laser energy density (Jmm^{-3}), P is the laser power (W), V is the scanning rate (mms^{-1}) d is the scan spacing (mm) and h is the layer thickness (mm). The relationship above shows that the energy density for the laser sintering process increases

with increasing laser power, and decreasing scanning rates, scan spacing and layer thickness.

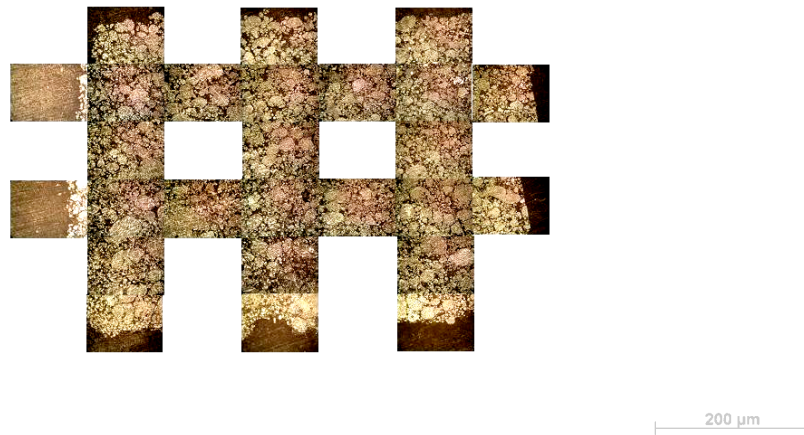Figure 6: Sections through the micrograph of AL-5 (200 W-120 mms^{-1}) generated by 67 Jmm^{-3}

Figure 7: Sections through the micrograph of AL-5 (150 W-120 mms^{-1}) generated by 50 Jmm^{-3}.

Therefore, plausible explanation for the observation noted in the values of sintered density when employing varying scanning rates and laser power (Figure 2) could be attributed to the optimisation of the energy density applied to the sintering process. As the energy density dissipated to the Al-12Si powder bed increases, the amount of liquid phase available for the densification mechanism increases until a critical value of energy density is reached. After the attainment of the critical energy density, further increament in the applied energy density results in spherodisation due to the oxidation of the Al-12Si powder particles. Moreover, spherodisation occurs owing to longer powders' particles exposure at high powder bed temperature. Spherodisation inhibits interparticulate bonding across the layers, thereby promoting the formation of porosity. Therefore, since spherodisation has crept in, the sintered densities of the samples are less than that

obtained at the critical energy density when the energy density is increased beyond its critical value. This explanation will now be applied to Figure 9.
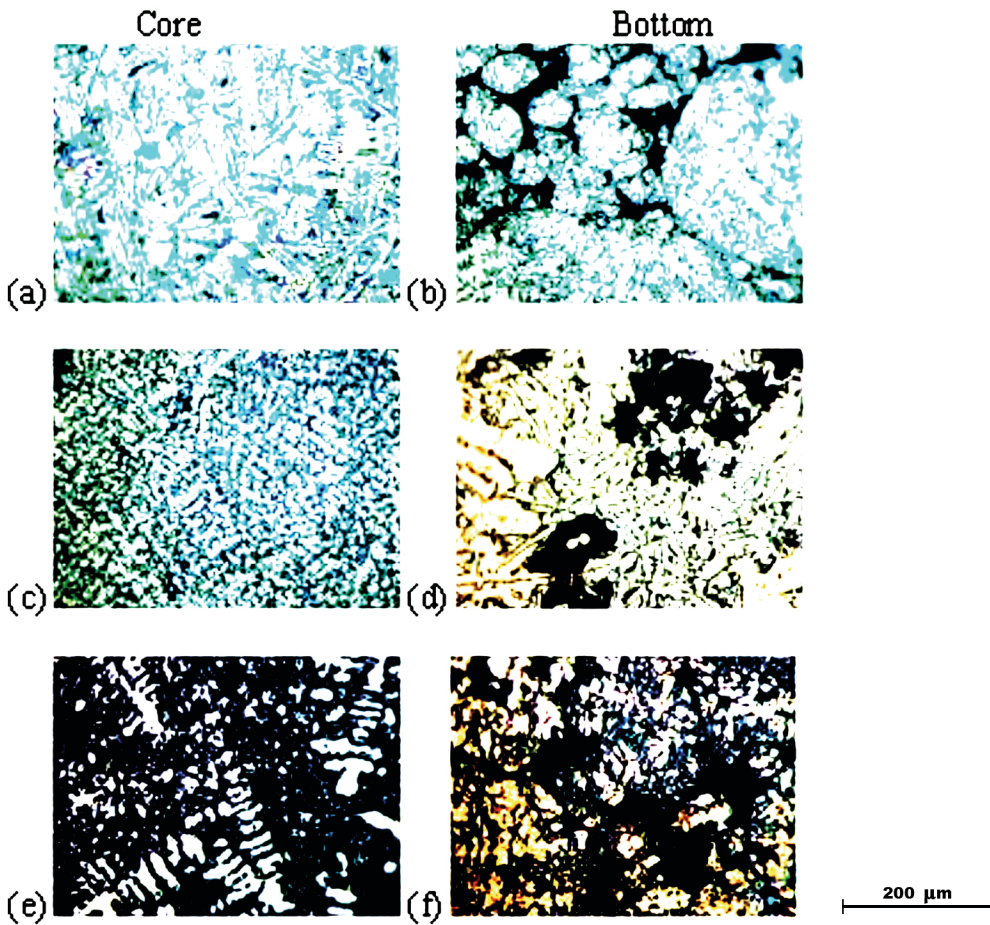

Figure 8: Optical micrographs show characteristic microstructures of direct laser sintered Al-12Si powder with varying processing conditions: (a, b) laser power 200 W; scan rates 80 mms^{-1}; layer thickness 0.25 mm; and scan spacing 0.1 mm (c, d) laser power 200 W; scan rates 120 mms^{-1}; layer thickness 0.25 mm; and scan spacing 0.1 mm (e, f) laser power 100 W; scan rates 80 mms^{-1}; layer thickness 0.25 mm; and scan spacing 0.1 mm.

Figure 9 shows that the sintered density of sample Al-12Si powder increases as the quantity of laser energy delivered to the powder bed increases until a critical energy density (optimum energy density) is attained. The maximum sintered density (80.2%) was obtained at this critical energy density of 67 Jmm^{-3} (corresponding to laser power 200 W; scan rates 120 mms^{-1}; scan spacing 0.1 mm; and layer thickness 0.25 mm). As the energy density is increased further, a gradual reduction in sintered density is observed until a point is reached when the sintered density remains unchanged (71.5%) despite further increases in energy density in the range 80-100 Jmm^{-3}. It is easily discernible at this stage that the reduction in the sintered density of Al-12Si powder observed between 80-100 Jmm^{-3} is consequent upon the initiation of spherodisation of Al-12Si powder particles as a result of exposure to higher bed temperature at the stated energy densities

307

for a longer duration. This occurs after the energy density has been optimised. Moreover, insufficient densification observed in the microstructures of direct SLS of Al-12Si powder below the critical value can be explained on the basis of the laser energy density reducing the amount of liquid phase available for sintering. This results in increased porosity and a reduction in the sample density.
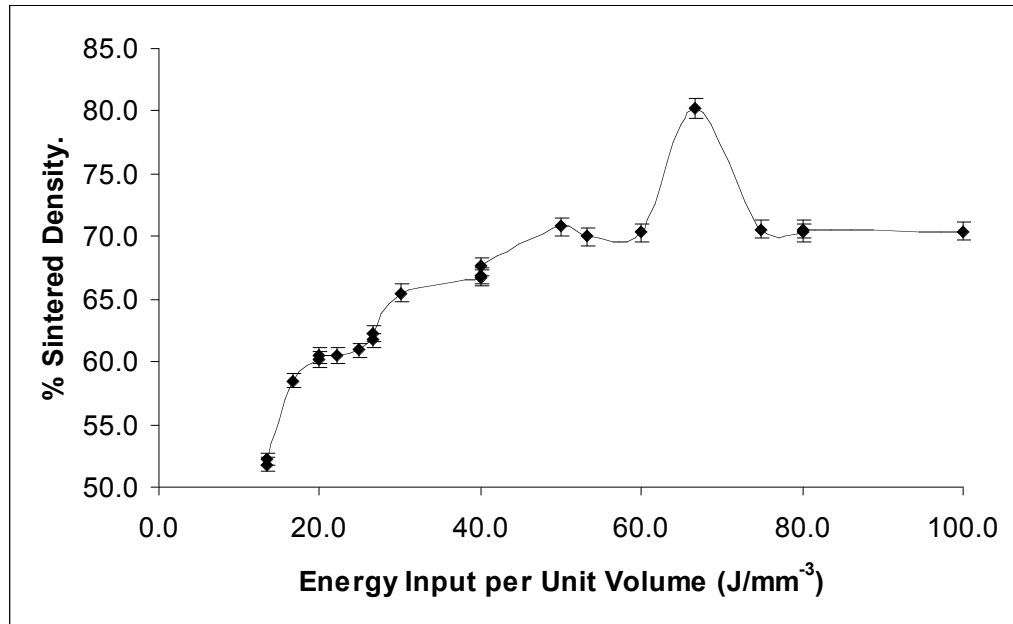

Figure 9: Graph of % apparent density versus the energy input per unit volume for Al-12Si aluminium powders for all processing conditions investigated.

The direct SLS technique employs a very high power density laser beam which is capable of generating typical cooling rates of the order of 10^3 to 10^4 K/s [13-14]. The fine microstructure observed in direct laser sintered Al-12Si sample processed with 67 J/mm^3 is a consequence of this high cooling rate. The implication of this is that the nature of the microstructure observed when varying laser power, scanning rates, scan spacing and layer thickness is dependent on the duration of the interaction between Al-12Si powder and the laser beam. The relationship between energy density and duration of laser-material interaction defines the operational regime of the direct SLS process which results in a unique temperature gradient (G), solidification rate (R) and cooling rate (T = G.R). It was noted that increasing the ratio G/R results in gradual change in the solidification regime from dendritic to cellular dendritic and eventually to planar front growth [13]. Furthermore, a higher cooling rate (G.R) leads to greater undercooling thus producing more nuclei of finer grains. Hence, the parameters (G/R) and (G.R) control the microstructural features and determine the scale of the microstructure [14-16]. With regard to laser sintered Al-12Si samples processed at 100 Jmm^3, a longer interaction time encountered by Al-12Si powder due to the combination of lower scanning rate (80 mms$^-$^{1}) and higher laser power (200 W) leads to the delay in the initiation of solidification process. Consequently, the temperature of the substrate material rises and the temperature gradient of the interface and the cooling rate are reduced. This leads to the formation of

coarse dendritic microstructure (Figures 8 (a) and (b)). Considering the case of Al-12Si sample processed at the critical energy density of 67 Jmm^{-3}, made up of higher scanning rate (120 mms^{-1}) and high laser power (200 W), it is speculated that superheating is not as high and the average temperature gradient at the interface is high thereby leading to faster cooling rate which results in a finer microstructure (Figure 8 (c) and (d)). As the deposited energy density (50 Jmm^{-3}) is less than the critical value, the heat input is just sufficient to sinter Al-12Si powder particles which eventually results in higher surface tensions of the melt pool and formation of cylindrical geometry. The contact area between two such layers will be smaller thereby leading to poor heat conduction, low cooling rate and dendritic microstructure (Figure 8 (e) and (f)).

During laser sintering, cooling of the molten pool occurs via the substrate and the surrounding atmosphere. Initially, heat loss through the Al-12Si substrate layer 1 results in rapid cooling via the substrate rather than through convection and radiation. The consequence of this is the directional growth of the dendrites counter to the cooling direction. A careful observation of Figure 10 shows that it seems that the tops of the grains in the previous layer 1 are partially re-melted and then serve as nuclei leading to epitaxial growth counter to the cooling direction. This process is repeated for many consecutive layers until the heat loss via the substrate is no longer dominant during the solidification mechanism. Consequently, the addition of a new layer 2 of material to the pre-existing layer results in the solidification of the region on top of the pre-existing layer 1 upon re-heating, thus grain growth takes place in pre-existing solid layers of the sintered sample (Figure 10). As the sample height increases, heat conduction to the substrate reduces and the build temperature increases. Therefore, the temperature change as a consequence of re-heating in the region underneath the interface affects a larger part of the build. As a result, the microstructure in the bottom part of the build (Figures 8) becomes coarse and the differences between re-heating and solidification become insignificant because heat extraction to the substrate for the lower region is unaffected. The disappearance of layer bands in the Figures 5-7 when the energy density varies between 50-100 Jmm^{-3} could be attributed to the same reason.

4.0 Conclusions

(1) Laser power, scanning rates, scan spacing and layer thickness are found to control the densification and the resultant microstructural characteristics of the laser sintered Al-12Si parts.

(2) Sintered density increased as the energy density until a critical energy input per unit volume (67 Jmm^{-3}) was realised for which the optimum sintered density (80.2%) was obtained. Above the critical energy density a gradual reduction in density was noted to have occurred until a point is reached at which the sintered density remains unchanged with further increases in energy density.

(3) Parts made with an energy density of 50 Jmm^{-3} were characterised by interconnected porosity and a fine dendritic microstructure while parts fabricated with an energy density

of 100 Jmm^{-3} consists of a coarse dendritic microstructure with discontinuous, irregularly shaped pores surrounded by a fully dense aluminium-silicon matrix.
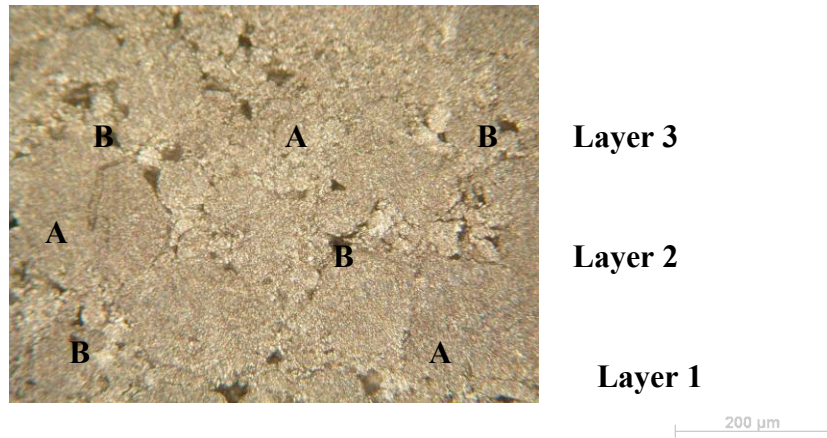

Figure 10: An enlargement of point 1 on the Figure 6 showing various points on the melt-back could be clearly observable across the layers (A) and areas where there had been no melt back resulting in porosity (B) during laser sintering.

References

[1] Niu, H. J. and I. T. H. Chang (1998). "Liquid phase sintering of M3/2 high speed steel by selective laser sintering." Scripta Materialia **39**(1): 67 - 72.

[2] Niu, H. J. and I. T. H. Chang (1999a). "Selective laser sintering of gas and water atomised high speed steel powders." Scripta Materalia **41**(1): pp. 25-30.

[3] Niu, H. J. and I. T. H. Chang (1999b). "Instability of scan tracks of selective laser sintering of high speed steel powder." Scripta Materalia **41**(11): pp. 1229-1234.

[4] Niu, H. J. and I. T. H. Chang (2000). "Selective laser sintering of gas atomized M2 high speed steel powder." Journal of Materials Science **35**: pp. 31- 38.

[5] Morgan, R. H., A. J. Papworth, et al. (2002). "High density net shape components by direct laser re-melting of single-phase powders." Journal of Materials Science **37**: pp. 3093 - 3100.

[6] Dewidar, M. M., K. W. Dalgarno, et al. (2003). "Processing conditions and mechanical properties of high-speed steel parts fabricated using direct selective laser sintering." in Proc. Instn. Mech. Engrs; J. Engineering Manufacture **217**(Part B): pp. 1651-1663.

[7] Sercombe, T. B. (2003b). "Sintering of freeformed maraging steel with boron additions." Materials Science and Engineering **A363**: pp. 242 - 252.

[8] Hauser, C., T. H. C. Childs, et al. (1999). <u>Selective laser sintering of stainless steel 314S HC processed using room temperature powder beds</u>. In Proc. Solid Freeform Fabrication Symposium., Austin, Texas.

[9] O'Neill, W., C. J. Sutcliffe, et al. (1999). "Investigation of multi-layer direct metal sintering of 316L stainless steel powder beds." <u>Annals CIRP</u> **48**(1): pp. 151.

[10] Fischer, P., V. Romano, et al. (2003). "Sintering commercially pure titanium powder with a Nd:YAG laser source." <u>Acta Materialia</u> **51**: pp.1651-1662.

[11] Fischer, P., V. Romano, et al. (2005). "Highly precise pulsed selective laser sintering of metallic powders." Laser Phys. Lett. **2,** No 1: pp.48-55.

[12] Srivastava, D., I.T.H.Chang, et al. (2001). "The effect of process parameters and heat treatment on the microstructure of direct laser fabricated TiAl alloy samples." <u>Intermetallics</u> **9** (12)**:** pp. 1003-1013.

[13] Steen, W.M. (1998) Laser Material Processing, Springer, Berlin.

[14] Basu, D., and Date, A.W.J., (1992). "Rapid solidification following laser melting of pure metals—I. Study of flow field and role of convection." <u>International Journal of Heat and Mass Transfer</u>, **35** (5): pp. 1049-1058.

[15] Loretto, M.H., A. B. Godfrey, et al., (1998). "The influence of composition and processing on the structure and properties of TiAl-based alloys." <u>Intermetallics</u>, **6** (7-8)**:** pp. 663-666.

[16] Srivastava, D., D. Hu., et al., (1999). "The influence of thermal processing route on the microstructure of some TiAl-based alloys" <u>Intermetallics</u>, **7** (10): pp. 1107-1112.